Published in Solar Wind Ten, AIP Conf. Proceedings 679, edited by M. Velli, R. Bruno, and F. Malara, p. 703-710, Melville, New York, 2003.

Models of Coronal Mass Ejections: A Review with A Look to The Future

Jon A. Linker*, Zoran Mikić*, Pete Riley*, Roberto Lionello* and Dusan Odstrcil†

*SAIC, 10260 Campus Point Dr., San Diego, CA 92121-1578, USA
†CIRES, University of Colarado, and NOAA/SEC, Boulder, CO 80305, USA

Abstract. Coronal mass ejections (CMEs) are a major transient input of mass and energy into the solar wind. We review some of the past and present concepts that influence the development of models of coronal mass ejections, both for CME initiation and CME evolution and propagation in the solar wind. We use the flux cancellation model to illustrate present research on CMEs. Primarily for convenience, modeling of CME propagation has usually been treated separately from the initiation problem. We suggest that future computational modeling of interplanetary CMEs is likely to emphasize the need to study coronal initiation and solar wind propagation together.

1. INTRODUCTION

Coronal mass ejections (CMEs) are dynamic, large-scale events in the solar corona that expel plasma and magnetic fields into the solar wind. CMEs typically appear as loop-like features that disrupt helmet streamers in the solar corona [1]. They were first observed with space-based coronagraphs in the early 1970's on OSO 7 [2] and Skylab [3]. Subsequent observations from the Solwind [4] and Solar Maximum Mission spacecraft [5] allowed identification of many of the properties of CMEs. The Solar and Heliospheric Observatory spacecraft has now extensively observed CME events from solar minimum in 1996 into the present maximum phase of the solar cycle. Halo events observed with the Large Angle Spectrometric Coronagraph (LASCO) [6, 7] now provide the most effective means of identifying earthward-directed CMEs, which are believed to be the primary cause of large, non-recurrent geomagnetic storms [8].

In situ signatures that are now recognized to be the interplanetary manifestations of CMEs have been measured for many years [9]. Perhaps the most frequently referred to example of an interplanetary CME is a magnetic cloud [10, 11] Magnetic clouds are identified in the solar wind as low beta plasmas associated with high field strength flux-rope structures; they are often (but not always) preceded by interplanetary shock waves [12]. While magnetic clouds are fairly common occurrences, many interplanetary structures that do not meet the criteria of magnetic clouds are also believed to be interplanetary CMEs. Other typical signatures of CMEs in the solar wind include counterstreaming suprathermal electrons [13] helium abundance enhancements [14] and low proton temperatures [15]. No single plasma or magnetic field characteristic is exhibited by all the structures identifed as interplanetary CMEs (see reviews by Gosling [16] and Neugebauer and Goldstein [17]).

Despite years of study, we still don't understand key aspects of CMEs; specifically, how are they initiated in the solar corona, and how they evolve to produce the signatures that are measured with interplanetary spacecraft. Clearly modeling must play a key role if we are to clarify these issues. There is a huge amount of literature on CMEs in general and CME modeling in particular, and we will not attempt to review the topic in detail. Rather, we show what some of the primary themes in CME modeling are today in the context of previous work, for both CME initiation and heliosphereic CME models. We briefly discuss the flux cancellation model as one of the present candidates for explaining CME initiation, and we discuss results obtained when the model is extended out into the interplanetary medium.

2. HOW ARE CMES INITIATED?

Models of CME initiation have been recently reviewed by Forbes [18], Klimchuk [19], and Low [20]; the reader is referred to these papers for a more comprehensive discussion. Our purpose here is to briefly outline the key issues regarding CME initiation, and what the likely direction of future research will be. CMEs can carry $> 10^{32}$ ergs of kinetic energy, so the most obvious question in studying this phenomena is where does the energy come from? Indeed, models of CME initiation can be broadly classified by their postulated energy source: (1)

Energy storage models; (2) energy driven models; (3) thermal blast models. (Note that [19] has a significantly more detailed classification scheme.) We will discuss types (2) and (3) first.

Energy driven models hypothesize that magnetic energy can be injected at a sufficiently rapid rate to drive an eruption directly. They have been proposed since the 1970s [21] but are in contradiction with a number of observations [18]. Driving a large CME directly requires on the order of 10^{32}ergs to be dumped into the corona in a few thousand seconds; the required Poynting flux implies magnitudes for photospheric motions of magnetic fields that are not observed [22]. Chen [23, 24] has proposed a flux injection mechanism that has similar energy requirements to these previous models. The model appears to describe coronal observations of CMEs in terms of flux ropes reasonably well [25], and also has been used to model interplanetary magnetic clouds [24]. However, the proposed initiation mechanism suffers from the same observational difficulties as previous energy driven models [19]

The thermal blast models were the earliest explanation for CMEs, and hypothesize that they are initiated by a sudden release of thermal energy in the lower corona from a solar flare [26, 27]. These models are similar to energy-driven models in that they require an impulsive energy release, and this is the only part of the CME process that is modeled. However, thermal blast models also assume that the energy for the flare was stored in the coronal magnetic field prior to the flare occurence. The thermal blast model appeared to be a plausible explanation for CMEs based on the initial discoveries of CMEs. However, subsequent observations have revealed numerous problems with this model as an explanation for the vast majority of CMEs; for example, less than about 20% of CMEs are associated with a large flare [8], and many flare-associated CMEs are initiated prior to the flare occurrence [28, 29].

Energy storage models are generally considered to be the most likely candidates at the present time. These models assume that the energy that drives CMEs and other forms of solar activity is stored slowly in the magnetic field prior to eruption. Highly non-potential coronal magnetic fields in active regions have been observed frequently [30, 31, 32, 33], indicating that there is more than enough magnetic energy to drive coronal eruptions. This energy may be stored by photospheric motions shearing and twisting the coronal field, or the magnetic fields may already be twisted when they emerge from below the photosphere. Present estimates indicate that most of the twist in active region magnetic fields actually emerges from below the photosphere when the regions are born [34]. In any case, how the magnetic energy is stored is not a critical feature of energy storage models. The key question for these models is how is this energy released.

Another constraint on CME models is that CMEs open (i.e., drag out into the solar wind) at least a portion of the coronal magnetic field. In strong magnetic field regions low in the corona, the magnetic field pressure dominates both the plasma pressure and the gravitational force, so that fields that are in equilibrium are essentially force-free. Aly [35, 36] and Sturrock [37] have shown that the energy of the *open field* (for a given magnetic flux distribution, the magnetic field with all field lines extending to infinity) is the maximum energy for a force-free magnetic field. This appears to present a paradox: how can the magnetic field be opened while releasing energy? CME models have been devised that circumvent this constraint in a variety of ways; for example, magnetic reconnection (the limit only applies to ideal MHD solutions) or by only partially opening the magnetic field.

CME initiation models are now progressing to the point that they can provide at least zero-order explanations for the energy release seen in coronal mass ejections as well as some of the qualitative features observed in white light (e.g., the LASCO coronagraph). As an example, we describe the flux cancellation model [38], in which converging flows near the neutral line causes the formation of flux ropes, which are a candidate structure for supporting prominences. Flux cancellation has been defined as the mutual disappearance of magnetic fields of opposite polarity at the neutral line separating them [39]. Observations have shown this process to be active at filament sites [40]. Calculations by Forbes and Isenberg [41] and Lin et al. [42] have suggested that once a flux rope is formed, continuation of the flux cancellation process can result in a loss of equilibrium. The new, lower energy equilibrium contains a current sheet and a higher height for the flux rope. In resistive MHD simulations, this current sheet is the site of rapid magnetic reconnection [43, 44, 45]. Figure 1 shows how a simulated helmet streamer configuration is disrupted by this process. The helmet streamer configuration shown has highly sheared magnetic field lines near the neutral line (see Linker et al. [45] for details), as is commonly observed in filament channels [46]. Flux cancellation first forms a stable flux rope configuration within the helmet streamer (2nd frame). The high density in the flux rope (seen in the white light image) is reminiscent of a prominence but because of the simplified (polytropic) energy equation, the plasma does not have the correct thermodynamic properties (it is too hot). (Linker et al. [44] have shown that when a more detailed energy equation is used, cool prominence-like material is lifted into the corona.) When flux cancellation continues, the helmet streamer is destabilized at $t_0 + 16$ hours (not shown) and subsequently erupts outward into the corona ($t_0 + 18$ and $t_0 + 20$ hours). The white light images show, albeit in a very idealized way, the 3 part structure often seen in CMEs.

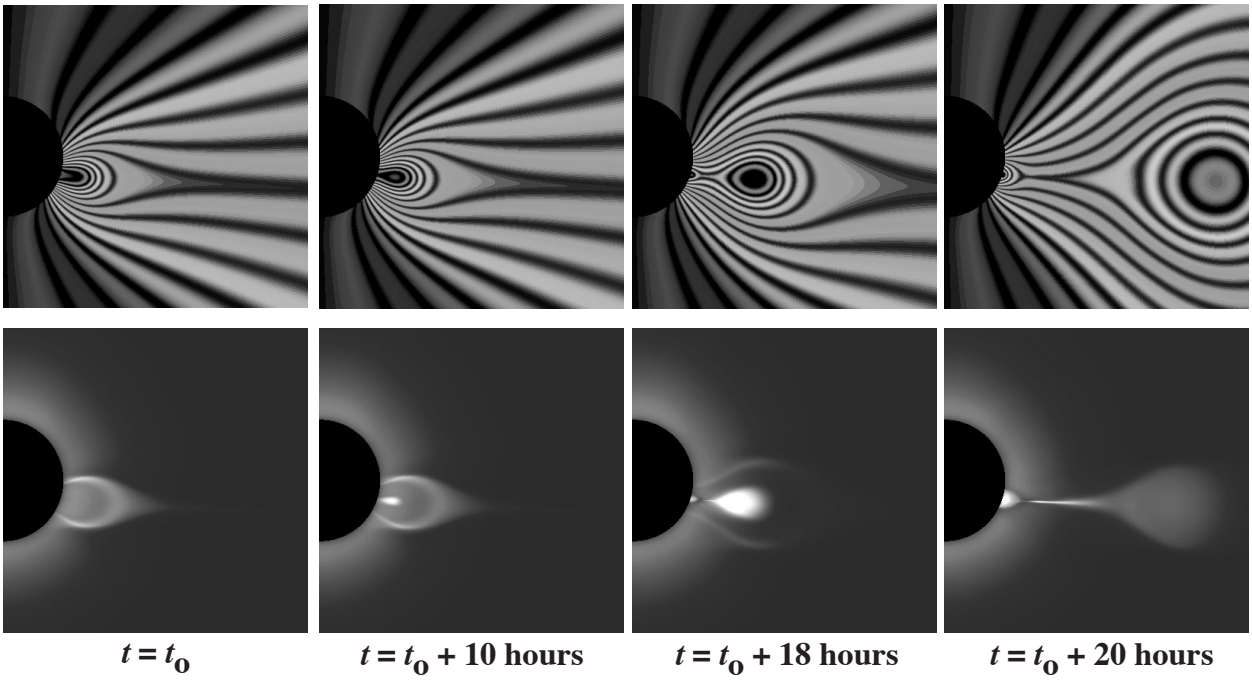

FIGURE 1. MHD Simulation of a helmet streamer eruption triggered by flux cancellation. The stripes in the top panels show projected field lines (there is also a component of the magnetic field, B_ϕ, out of the plane) and the bottom panels shows the polarization brightness that would be observed by a coronagraph if this were a real CME. At $t_0 + 10$ hours a high density flux rope has formed; this structure is stable if flux cancellation is halted. With continued flux cancellation, the configuration erupts.

The "breakout" model [47] is another viable initiation mechanism. It requires a multipolar flux distribution, and like the flux cancellation model, requires strongly sheared fields near the neutral line as is observed in filament channels. As shear in the central arcade is increased, slow reconnection transfers overlying flux in the central arcade to the neighboring arcades. As the restraining force of the overlying flux is decreased, the sheared field lines rises further, causing yet more overlying flux to be diverted. Eventually all of the overlying flux is removed and the sheared central arcade erupts explosively. While MHD simulations for the breakout model have not yet been performed on a more realistic helmet streamer configuration, they have demonstrated an explosive energy release.

Flux cancellation and breakout are two of the best developed models at the moment, but there are many others (including a recent model by Low and Zhang [48]). Why can't we tell which (if any) of these models is correct? In many cases the expected observational differences between the models are subtle. For example, flux cancellation requires a flux rope prior to eruption, while breakout does not. Distinguishing between field lines that wrap around each other ("flux rope") from a collection of strongly-sheared dipped field lines is quite difficult for realistic fields. We note that after eruption, the ejected material is expected to be embedded in a flux rope in both models. Indeed, both coronal and interplanetary observations indicate that some fraction of CMEs contain flux ropes, but unfortunately this information does not discriminate between any of the actively considered models. (Incidentally, this explains why the Chen [23] flux rope model, which appears to have untenable assumptions about CME energetics, can still model LASCO images of CMEs reasonably well.)

While breakout, flux cancellation, and other energy storage models can explain some aspects of the observations, so far they have only been studied for relatively idealized configurations. The challenging task for all CME models is to increase their sophistication to the point where calculations of specific events can be performed, and observable quantities, such as disk emission seen in Yohkoh soft X-ray images and SOHO Extreme ultraviolet Imaging Telescope (EIT) images, can be realistically predicted and tested against the observations. This is especially true for observations that will be available in the next few years (e.g., the Solar-B and STEREO missions).

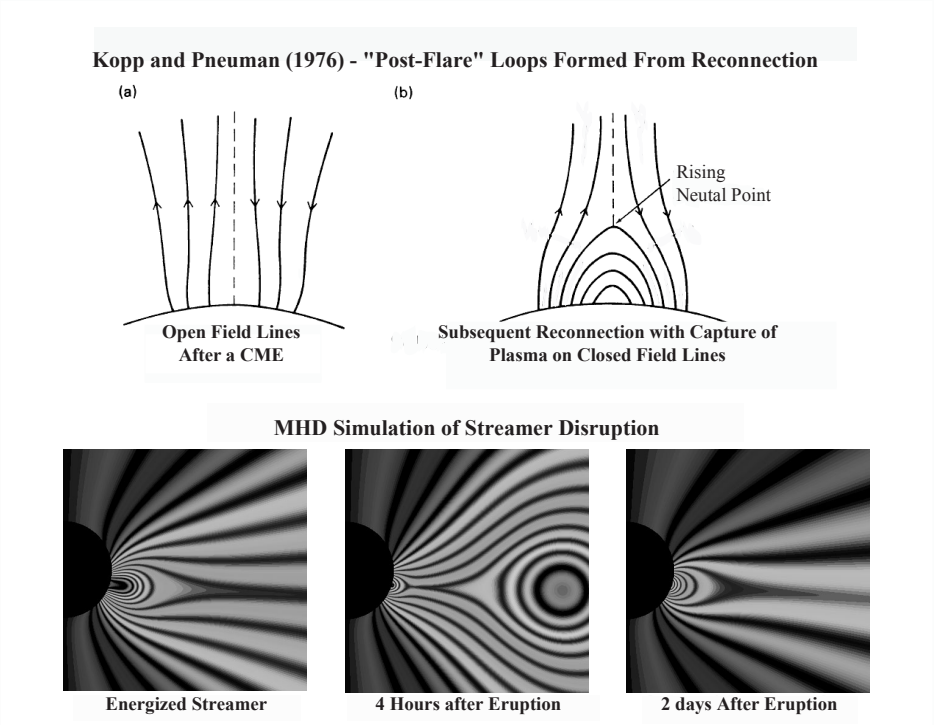

FIGURE 2. (a) (After Kopp and Pneuman [49].) Eruption opens previously closed magnetic field lines. (b) reconnection reforms the closed field, resulting in images of successively higher "postflare" loops. (c) Reformation of the helmet streamer in the aftermath of a CME (from the flux cancellation simulation of Figure 1).

3. WHAT WE THINK WE DO UNDERSTAND ABOUT CMES?

While the underlying cause of CMEs is unresolved, the eruption process in the corona has been documented by many observations. At least for the simplest mass ejections, a picture that began to emerge over 25 years ago reconciles a number of the observations. When CMEs disrupt helmet streamers, they open previously closed magnetic field regions (Figure 2a). Kopp and Pneuman [49] suggested that the reclosing of these magnetic fields led to the formation of the successivly higher "post-flare" loops seen in the aftermath of eruptive events (Figure 2b). The phenomenon has since been associated with CMEs [50]. MHD simulations of helmet streamer disruptions via flux cancellation show the formation of new loops in the aftermath of the eruptive process (Figure 2c). This effect appears to be independent of the mechanism that disrupts the helmet streamer; for example, the post-eruptive loop formation is seen in simulations of CMEs initiated by photospheric shearing flows [51]. The well known observation of bands moving away from the neutral line in two-ribbon flares observed in Hα [52] is explained by this mechanism as the reconnection line at the top of the arcades moving upward. As the arcades reform and increase in size, the Hα ribbons (bounding the arcades) move outward.

Figure 3 shows an example of post-eruption loop formation for the CME event of September 12, 2000. In the pre-event state, a prominence is seen in both EUV and Hα. A halo CME was subsequently observed in the LASCO C2 and C3 coronagraphs, during which time the formation of the post-eruption loops were observed in EIT and Yohkoh.

4. CME EVOLUTION IN THE SOLAR WIND

Until recently, most multi-dimensional models of interplanetary CMEs in the solar wind eliminated the inner corona from consideration by starting at $20-40R_s$ (beyond the Alfvén and sonic points in the corona). This approach enormously simplifies the inner boundary condition; beyond these critical points the MHD characteristics all point into the computational domain and the upstream quantities can be arbitrarily specified. The earliest studies looked at the propagation of interplanetary shockwaves [53, 54] based on the "thermal blast" model of CMEs (see section 2). Later models recognized

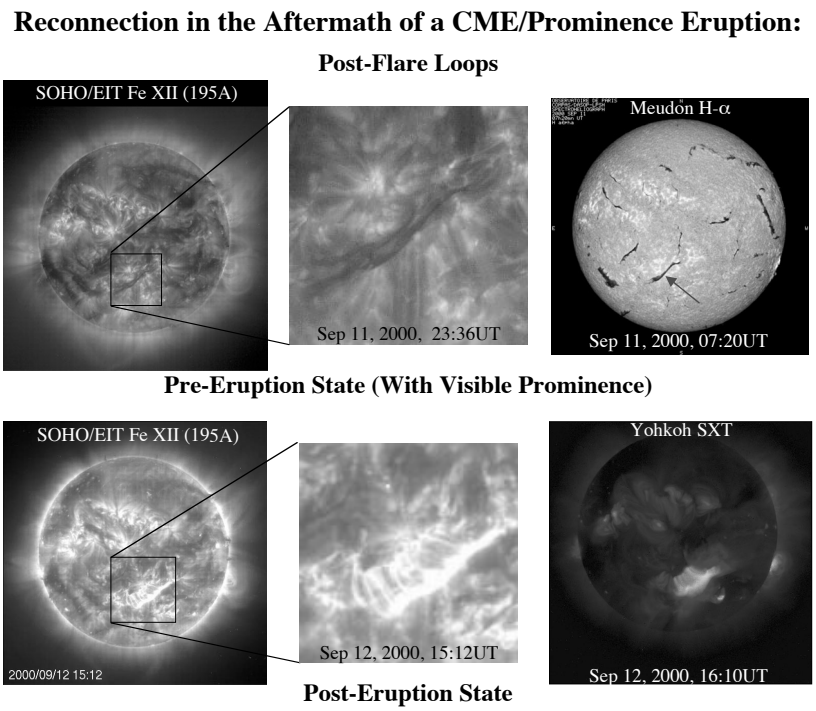

FIGURE 3. Pre- and post event images for the September 12,2000 CME. (a) EIT and Hα images of a filament prior to eruption. The red arrow in the Hα image indicates the position of the filament. (b) EIT and Yohkoh images of the post-eruptive state, showing the presence of post-eruption loops after the disappearance of the filament. During this time the CME was observed in LASCO images.

the importance of the magnetic topology of the CME and investigated the propagation of spheromak structures and cylindrical flux ropes [55, 56, 57], including models of the localized effects of propagation on the flux-rope structure [58]. Riley et al. [59] and Odstrcil and Pizzo [60, 61] investigated the effects of solar wind velocity structure on CME ejecta, using an idealized density pulsed injected into a two-state (fast and slow) solar wind. Odstrcil and Pizzo [62] also investigated how the background solar wind magnetic field is affected by the ejecta. The complicated density structures that emerged from these calculations show the richness of behavior that is possible.

While models that provide solutions beyond the critical points have instructed us about important aspects of CME propagation, the properties of the CME ejecta in these calculations are somewhat arbitrary. By definition, these models cannot directly connect the initiation of a CME with the subsequent interplanetary observations, this requires a calculation starting at the Sun. Such calculations have already been performed. The three-dimensional (3D) computation by Linker and Mikić [63] showed how differential rotation on the Sun can eventually disrupt a helmet streamer, ejecting a portion of the streamer belt out into the solar wind. Wu et al. [64] performed a 2D calculation that followed the evolution of a simulated helmet streamer eruption from the corona out to Earth orbit, and Groth et al. [65] performed a 3D computation that included the interaction of the simulated CME with the Earth's magnetosphere. All of these models were useful for demonstrating both CME initiation and propagation in a single calculation, but the initiation mechanisms themselves were not very realistic. The differential rotation studied by Linker and Mikić [63] is unlikely to be a major source of energization for coronal magnetic fields. The Wu et al. [64] model imposed an ad hoc increase of the magnetic field perpendicular to the plane of the computation (B_ϕ in spherical coordinates) for an arbitrarily specified portion of the grid; this created a flux rope that eventually disrupted the helmet streamer [66]. Groth et al. [65] relied on a pressure pulse similar to the earlier thermal blast models.

Ideally, we would like the calculations of CME initiation described in section 2 to be extended out into the solar wind; solar wind measurements might possibly then provide another test of the proposed initiation mechanisms. As a demonstation of this idea, Odstrcil et al. [67] have coupled the SAIC coronal model with the

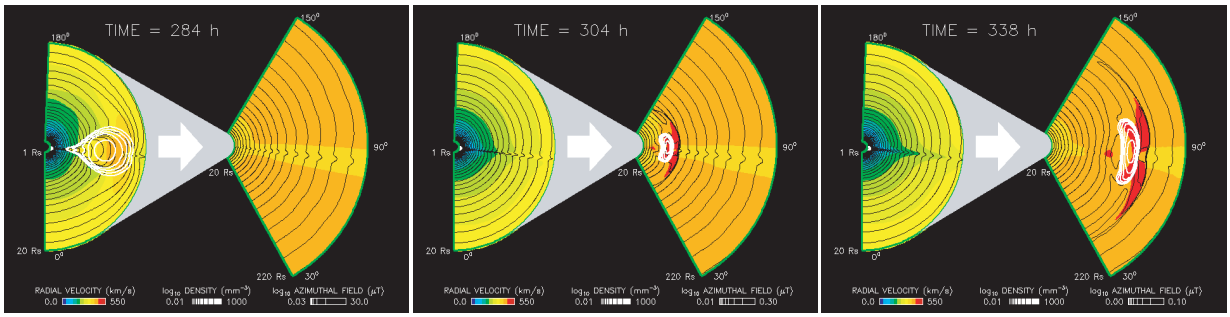

FIGURE 4. Computation of a CME initiated by flux cancellation out to 1 A.U., using the coupled SAIC and NOAA/SEC MHD models. In each frame, the leftmost hemisphere shows the domain of the coronal simulation, which feeds into the heliospheric simulation (wedge-shaped domain on the right). Black lines show contours of density. Colors show the solar wind speed. White lines show contours of B_ϕ and mark the approximate location of the flux rope. The region of highest velocity (red) and density pileup show the location of the shockwave.

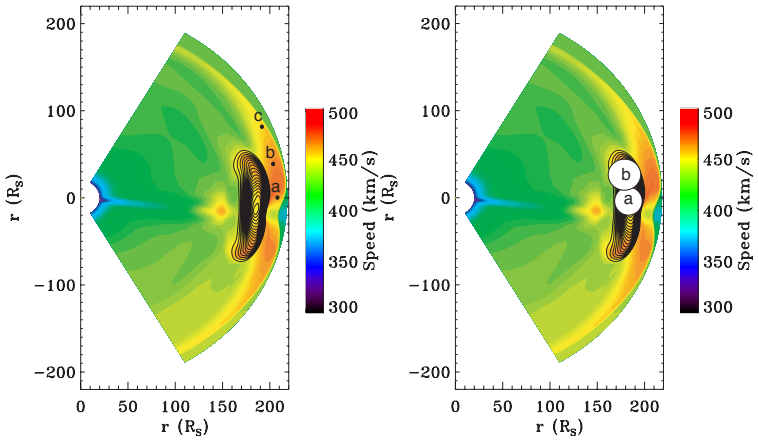

FIGURE 5. In the left frame, the simulated CME near 1 A.U. (from the same calculation of Figure 4) is shown together with a color map of the solar wind speed. Black lines are contours of B_ϕ and show the location of the flux rope. The positions of hypothetical spacecraft that encounter the simulated CME are marked a, b, and c. The right frame is the same as the left, but the white circles show the size and shape of the flux ropes inferred by fits to a linear force-free (LFF) model.

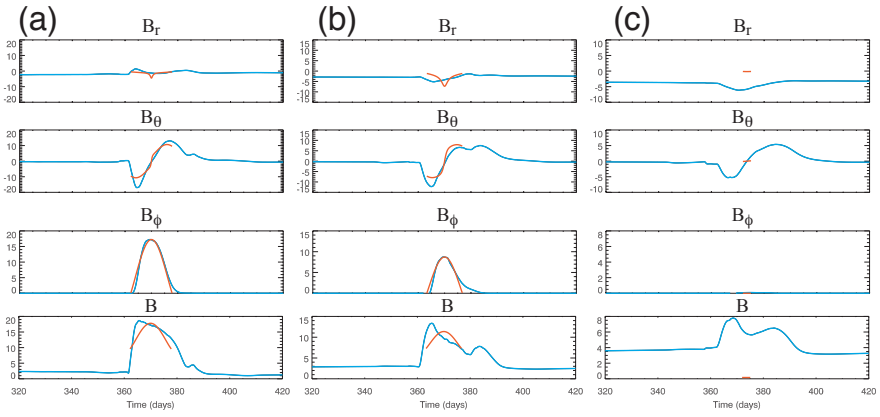

FIGURE 6. The time series of the magnetic field (blue lines) as "measured" by the hypothetical spacecraft a, b, and c in Figure 5. The field resulting for a best fit to a linear force free cylindrical flux rope is shown in red; the inferred flux ropes are the white circles shown in Figure 5.

NOAA/SEC heliospheric model to extend the flux cancellation simulation of Figure 1 out to 1 A.U. Figure 4 shows results from these coupled models. On the left of each frame, the domain of the coronal model is shown while on the right the domain of the heliospheric model is depicted. The simulation shows that a flux rope (identified by the white contours showing the concentration of B_ϕ) propagates outward. Close to the Sun the shape of the flux rope is nearly circular but it becomes wedge-shaped as it drives into the ambient slower solar wind; this is accompanied by the formation of a fast mode shockwave ahead of the ejecta.

The calculation of Figure 4 is highly idealized, nevertheless it shows that even the simple propagation of a flux rope can lead to the formation of a relatively complex structure. It is interesting to investigate how data for this simulated flux rope might be appear for spacecraft situated in different locations. The leftmost frame of Figure 5 shows the plasma speed as a color map and the position of the flux rope (black contours) when the CME is near Earth orbit. (The rightmost frame of Figure 5 is discussed below.) The position of three hypothetical spacecraft (a,b,c) is also shown. At this point in time, the shockwave has just passed over all of the spacecraft. Spacecraft (a) and (b) are about to encounter the simulated CME ejecta. The blue curves in Figure 6 shows the simulated time series of the magnetic field "measured" by the three spacecraft.

Linear (constant α) force-free field models are frequently found to give good fits to interplanetary flux ropes [68]. We derived a fit to a simple linear force-free (LFF) model to the time series of data observed by each hypothetical spacecraft. The red lines in Figure 6 show the results of this fitting procedure. The LFF model finds quite a good fit to the magnetic field for the time series from spacecraft (a), and the model also finds a reasonable fit for the data from spacecraft (b). Spacecraft (c) misses the flux rope entirely and the LFF model correctly finds no fit. This simple LFF model assumes a cylindrical flux rope shape, a frequent assumption of the models used to interpret interplanetary data. The white circles in the rightmost frame of Figure 5 show the position and shape of the flux ropes inferred by the LFF model. We see that the sizes and shapes of the inferred flux ropes are very misleading, despite the fact that reasonable fits were obtained. Our results indicate that one needs to be careful about assuming that flux ropes are actually cylindrical, even if a cylindrical model gives a good fit to the data. Non-force free [69] or noncylindrical [70] approaches might yield a more accurate description of the shape. Given the relative simplicity of this idealized MHD simulation, one can easily imagine why in the real solar wind, CME ejecta can develop far more complicated configurations. MHD simulations may help to give us insights into the best way to utilize measurements of these structures. Interplanetary observations in turn provide an important test of CME models.

5. SUMMARY

Modeling of CMEs has traditionally been separated into coronal calculations that primarily focus on CME initiation, and heliospheric models that focus on interplanetary evolution of CMEs. Solving the puzzle of CME genesis will likely require more sophisticated CME simulations that can be applied to specific events. As CME initation models are driven to more realism in order to confront the detailed coronal images we now obtain in a variety of wavelengths, the natural course is to also extend the initiation models into interplanetary space. We have shown here an example for flux cancellation, a candidate initiation mechanism. Coupled initiation and interplanetary propagation models of CMEs are likely to increase in sophistication in the near future.

Acknowledgments

The images in Figure 3 are from the EIT instrument aboard the SOHO spacecraft, the Yohkoh soft X-ray telescope, and the spectroheliograph at Meudon observatory. This work was supported by NASA's SR&T, LWS, and SECTP programs, and by NSF grants ATM0000950 and ATM0120950 (The Center for Integrated Space Weather Modeling). Computations were performed at the San Diego Supercomputer Center. We also wish to acknowledge beneficial discussions at the SHINE workshops.

REFERENCES

1. Hundhausen, A. J., *J. Geophys. Res.*, **98**, 13,177, 1993.
2. Tousey, R., *Bull. Amer. Astronom. Soc.*, **5**, 419, 1973.
3. MacQueen, R. M., Eddy, J. A., Gosling, J. T., Hildner, E., Munro, R. H., Newkirk, G. A., Jr., Poland, A. I., and Ross, C. L., *Astrophys. J.*,**187**, L85, 1974.
4. Michels, D. J., Howard, R. A., Koomen, M. J., and Sheeley Jr., N. R., in *Radio Physics of the Sun*, ed. by M. R. Kundu and T. Gergely, D. Reidel, Hingham, MA, 1980, p. 439.
5. MacQueen, R. M., Csoeke-Poeckh, A., Hildner, E., House, L., Reynolds, R., Stanger, A., Tepoel, H., and Wagner, W., *Solar Phys.*, **65**, 91, 1980
6. Brueckner, G. E., Howard, R. A., Koomen, M. J., Korendyke, C. M., Michels, D. J., Moses, J. D., Socker, D. G., Dere, K. P., Lamy, P. L., Llebaria, A., Bout, M. V., Schwenn, R., Simnett, G. M., Bedford, D. K., Eyles, C. J., *Solar Phys.*, **162**, 375, 1995.
7. Howard, R. A., et al., in Coronal Mass Ejections (N. Crooker, J. Joselyn and J. Feynman, eds.), *Geophys. Monogr.*, **99**, 17, 1997.

8. Gosling, J. T., *J. Geophys. Res.*, **98**, 18,937, 1993.
9. Gosling, J. T., Pizzo, V., Bame, S., *J. Geophys. Res.*, **78**, 2001, 1973.
10. Burlaga, L., Sittler, E., Mariani, F., Schwenn, R., *J. Geophys. Res.*, **86**, 6,673, 1981.
11. Klein, L. W., Burlaga, L. F., *J. Geophys. Res.*, **87**, 613, 1982.
12. Marubashi, K., in Coronal Mass Ejections (N. Crooker, J. Joselyn and J. Feynman, eds.), *Geophys. Monogr.*, **99**, 147, 1997.
13. Gosling, J. T., Thomsen, M. F., Bame, S. J., Zwickl, R. D., *J. Geophys. Res.*, **92**, 12,399, 1987.
14. Borini, G., Gosling, J. T., Bame, S. J., Feldman, W. C., *J. Geophys. Res.*, **87**, 7,370, 1981.
15. Richardson, I. G., and Cane, H. V., *J. Geophys. Res.*, **100**, 23,397, 1995.
16. Gosling, J. T., in Coronal Mass Ejections (N. Crooker, J. Joselyn and J. Feynman, eds.), *Geophys. Monogr.*, **99**, 9, 1997.
17. Neugebauer, M., Goldstein, R., in Coronal Mass Ejections (N. Crooker, J. Joselyn and J. Feynman, eds.), *Geophys. Monogr.*, **99**, 245, 1997.
18. Forbes, T. G., *J. Geophys. Res.*, **105**, 23,153, 2000.
19. Klimchuk, J. A., in *Space Weather*, ed. by P. Song, H. Singer, and G. Siscoe, *Geophys. Monogr.*, **125**, AGU, Washington, 2001, p. 143.
20. Low, B. C., *J. Geophys. Res.*, **106**, 25,141, 2001.
21. Heyvaerts, J., *Sol. Phys.*, **38**, 419, 1974.
22. McClymont, A. N., Fisher, G. H., in Solar System Plasma Physics, (J. H. Waite, J. L. Burch, and R. L. Moore, eds.), *Geophys. Monogr.*, **54**, 219, 1989.
23. Chen, J., *Astrophys. J.*, **338**, 453, 1989.
24. Chen, J., *J. Geophys. Res.*, **101**, 27,499, 1996.
25. Chen, J., Howard, R. A., Brueckner, G. E., Santoro, R., Krall, J., Paswaters, S. E., St. Cyr, O. C., Schwenn, R., Lamy, P., Simnett, G. M., *Astrophys. J.*, **490**, L191, 1997.
26. Dryer, M., *Space Sci. Rev.*, **33**, 233, 1982.
27. Wu, S. T., *Space Sci. Rev.*, **32**, 115. 1982.
28. Harrison, R. A., *Astron. and Astrophys.*, **162**, 283, 1986.
29. Hundhausen, A. J., in Proceedings of the Sixth International Solar Wind Conference (Solar Wind 6) (V. J. Pizzo, T. E. Holzer, and D. G. Sime, eds), NCAR/TN-306+Proc, Boulder, 181, 1988.
30. Gary, G. A., Moore, R. L., Hagyard, M. J., Haisch, B. M. , *Astrophys. J.*, **314**, 1987.
31. Hagyard, M. J., *Sol. Phys.*, **115**, 1988.
32. Canfield, Richard C., de La Beaujardiere, J.-F., Fan, Y., Leka, K. D., McClymont, A. N., Metcalf, T. R., Mickey, D. L., Wuelser, J-P., Lites, B. W., *Astrophys. J.*, **411**, 362, 1993.
33. Leka, K. D., Canfield, Richard C., McClymont, A. N., de La Beaujardiere, J.-F., Fan, Y., and Tang, F., *Astrophys. J.*, **411**, 370, 1993.
34. Démoulin, P., Mandrini, C. H., van Driel-Gesztelyi, L., Thompson, B. J., Plunkett, S., Kovári, Z., Aulanier, G., Young, A., *Astron. and Astrophys.*, **382**, 2002.
35. Aly, J. J., *Astrophys. J.*, **283**, 349, 1984.
36. Aly, J. J., *Astrophys. J.*, **375**, 61L, 1991.
37. Sturrock, P. A., *Astrophys. J.*, **380**, 655, 1991.
38. van Ballegooijen, A. A., and Martens, P. C. H., *Astrophys. J.*, **361**, 971, 1989.
39. Martin, S. F., S. H. B. Livi, and Wang, J., *Australian J. Phys.*, **38**, 929, 1985.
40. Litvinenko, Y. E., Martin, S. F., *Solar Phys.*, **190**, 45, 1999.
41. Forbes, T. G., Isenberg, P. A., *Astrophys. J.*, **373**, 294, 1991.
42. Lin, J., Forbes, T. G., Isenberg, P. A., Démoulin, P., *Astrophys. J.*, **504**, 1,006, 1998.
43. Amari, T., Luciani, J. F., Mikić, Z., and Linker, J., *Astrophys. J.*, **529**, 49L, 2000.
44. Linker, J. A., Lionello, R., Mikić Z., and Amari, T., *J. Geophys. Res.*, **106**, 25165, 2001.
45. Linker, J. A., Mikić Z., Lionello, R., Riley, P., Amari, T., and Odstrcil, D., *Phys. Plasmas*, to appear, 2003.
46. Martin, S. F., and C. R. Echols, in *Solar Surface Magnetism*, ed. by R. J. Rutten and C. J. Schrijver, Kluwer Academic, Dordrecht, Netherlands, 1994, p. 339.
47. Antiochos, S. K., MacNeice, P. J., Spicer, D. S., and Klimchuk, J. A., *Astrophys. J.*, **512**, 985, 1999.
48. Low, B. C., Zhang, M., *Astrophys. J.*, **564**, L53, 2002.
49. Kopp, R. A., Pneuman, G. W., *Solar Phys.*, **50**, 85, 1976.
50. Hiei, E., Hundhausen, A. J., Sime, D. G., *Geophys. Res. Lett.*, **20**, 2,785, 1993.
51. Linker, J. A., Mikić, Z., *Astrophys. J.*,**438**, L45, 1995.
52. Zirin, H., *Astrophysics of the Sun*, Cambridge, 1988.
53. Wu, S. T., Dryer, M., Han, S. M., *Solar Phys.*, **84**, 395, 1983.
54. Dryer, M., *Space Sci. Rev.*, **67**, 363, 1994.
55. Detman, T. R., Dryer, M., Yeh, T., Han, S. M., Wu, S. T., *J. Geophys. Res.*, **96**, 9,531, 1991.
56. Vandas, M., Fischer, S., Dryer, M., Smith, Z., and Detman, T., *J. Geophys. Res.*, **101**, 2505, 1996.
57. Vandas, M., Fischer, S., Dryer, M., Smith, Z., and Detman, T., *J. Geophys. Res.*, **101**, 15,645, 1996.
58. Cargill, P. J., Chen, J., Spicer, D. S., Zalesak, S. T., *J. Geophys. Res.*, **101**, 4,855, 1996.
59. Riley, P., Gosling, J. T., and Pizzo, V. J., *J. Geophys. Res.*, **102**, 14,677, 1997.
60. Odstrcil, D., Pizzo, V., *J. Geophys. Res.*, **104**, 483, 1999.
61. Odstrcil, D., Pizzo, V., *J. Geophys. Res.*, **104**, 493, 1999.
62. Odstrcil, D., Pizzo, V., *J. Geophys. Res.*, **104**, 28,225, 1999.
63. Linker, J. A., Mikić, Z., in *Coronal Mass Ejections*, ed. by N. Crooker, J. Joselyn and J. Feynman, *Geophys. Monogr.*, **99**, AGU, Washington, 1999, p.269.
64. Wu, S. T. Guo, W. P., Michels, D. J., Burlaga, L. F., *J. Geophys. Res.*, **104**, 14,789, 1999.
65. Groth, C. P. T., de Zeeuw, D. L., Gombosi, T. I., Powell, K. G., *J. Geophys. Res.*, **105**, 25,053, 2000.
66. Wu, S. T., Guo, W. P., in Coronal Mass Ejections (N. Crooker, J. Joselyn and J. Feynman, eds.), *Geophys. Monogr.*, **99**, 83, 1997.
67. Odstrcil, D., Linker, J. A., Lionello, R., Mikić, Z., Riley, P., Pizzo, V. J., and Luhmann, J., *J. Geophys. Res.*, **107**, 10.1029/2002JA009334, 2002.
68. Lepping, R. P., Burlaga, L. F., Jones, J. A., *J. Geophys. Res.*, **95**, 11,957, 1990.
69. Hidalgo, M. A., Cid, C., Medina, J., Viñas, A. F., *Solar Phys.*, **194**, 165, 2000.
70. Mulligan, T, Russell, C. T., *J. Geophys. Res.*, **106**, 10,581, 2001.